DOI: https://doi.org/10.36094/sc.v89.2025.Electrical_Resistance_Properties_of_In_House.Hussain.56

ARTICLE

Sci. and Cult. 91 (1–2) : 56-61 (2025)

ELECTRICAL RESISTANCE PROPERTIES OF *IN-HOUSE* PREPARED SAMARIUM TITANATE ($Sm_2Ti_2O_7$) FOR HIGH TEMPERATURE SENSOR APPLICATION

NAIMUR HUSSAIN[3], P.K. PANDA[1], B.W. SHIVARAJ[2] AND P. SIVAGNANAPALANI[1]*

Samarium titanate (STO), with $Sm_2Ti_2O_7$ structure, stands out among perovskite-like layered materials due to its impressive thermal stability and high Curie temperature (Tc). These properties make STO an excellent candidate for high-temperature sensor applications and capable of functioning effectively up to 1250 °C. In the present study, the samarium titanate (STO) powders were synthesized by solid-state reaction method. These powders were used to prepare thin tapes by tape casting method. This technique is more advantageous for making miniaturized sensors due to its ability to produce uniform and thin layers of material. The resulting tapes were then stacked and subjected to sintering at 1450 °C for two hours. The samples were characterized for their suitability as high temperature sensor applications. The study also includes measuring and comparing the electrical resistivity of both bulk form samples and those prepared by tape casting method. The comparative study provided insights into the advantages of using tape-cast STO in sensor technology.

Keywords: *Samarium titanate (STO), Tape casting, high temperature sensors, Perovskite-like layered (PLS), Resistivity*

Introduction

In aero-engines and gas turbines, where operational temperatures often cross beyond 1000°C, hence there is need for reliable and precise temperature measurement devices is important[1]. These systems demand sensors that not only withstand extreme conditions but also measure accurate readings to ensure optimal performance and safety. In recent times, the temperature sensor technology has evolved significantly, incorporating various methods such as thermographic phosphors, surface acoustic wave (SAW) sensors, thermocouples and resistance temperature detectors (RTD) have been used to measure high temperatures[2-4]. Polymer-derived composites (PDC) based thin films are used as temperature sensors due to their high thermal stability[5]. The existing sensors experience accuracy loss and poor response times due to material properties, thermal quenching, and drifts, which limit these techniques[3,6-8]. These challenges necessitate the exploration of alternative materials that can overcome these drawbacks.

The perovskite-like layered structure (PLS) exhibits high Curie temperatures (T_c) and is a stable material for high-temperature sensor applications. These materials, with composition $A_2B_2O_7$ (A = Sr, Ca, La, Nd and B = Nb, Ti) shows remarkable ferroelectric properties[9]. Numerous studies have been carried out on the piezoelectric properties of PLS materials and their super high Curie

1 Materials Science Division, CSIR-National Aerospace Laboratories, Bengaluru 560017, India

2 Department of Mechanical Engineering, Vivekananda Institute of Technology, Bengaluru 560074, India

3 Department of Mechanical Engineering, R.V. College of Engineering, Bengaluru 560059, India

* Corresponding Author: psiva@nal.res.in

temperatures (Tc)[10-12]. Furthermore, extensive research has been carried out to study the ferroelectric properties and electrical resistivity at high temperatures for PLS materials such as $Sr_2Nb_2O_7$ (SNO), $Ca_2Nb_2O_7$ (CNO), $La_2Ti_2O_7$ (LTO), $Nd_2Ti_2O_7$ (NTO) and $Sm_2Ti_2O_7$ (STO)[13-17]. However, all the above studies were focused on only bulk materials.

To achieve this, the above mentioned materials need to be implemented in the form of thin films. This can be accomplished by different coating techniques such as thermal spray coating, sputter coating, plasma spray coating, and wet chemical coatings[18]. One of the effective technique for fabricating ceramic thin films is by tape casting method, which are widely used in substrates, capacitors, and sensors[19-21]. This method offers the flexibility to produce tapes of various thicknesses[22]. The tape casting process involves preparation of slurry by mixing the powders, solvents, binders, plasticizer, and dispersants. The slurry is then poured onto a moving conveyor belt where it passes through a doctor blade to form a thin layer (micron thickness). Significant advancements have been made using the tape casting method, such as the fabrication of multi-layered lead zirconate titanate (PZT) based actuators and biomorphs for energy harvesting[23]. Moreover, the researchers have successfully developed electrochemical gas sensors with a thin tape-cast layer of yttria-stabilized zirconia (YSZ) as the electrolyte to which the electrodes are attached [24,25]. Spitsin et al. had developed the innovative applications of a multilayered piezo stack of $Na_{0,5}Bi_{4,5}Ti_4O_{15}$ (NBT) using tape casting technology, which is a high curie temperature (T_c = 645 °C) lead-free ceramic[26]. The NBT stack exhibited a remarkable density of 97%, indicating superior dielectric characteristics. In the present study, efforts have been carried out to develop samarium titanate (STO) powder using the solid-state reaction process, and to fabricate micron size tapes by tape casting method. The tapes will be subsequently sintered and characterized for their suitability in high temperature sensor applications.

Materials and Methods

Sample Preparation: **Preparation of Samarium Titanate Powders:** Samarium titanate powders were prepared by mixed oxide method using high-purity samarium oxide (99.9% purity, Loba Chemie, India) and titanium dioxide (99.8% purity, Merck, US) as precursor materials. The mixed powders underwent a 6-hour planetary milling process in an ethanol medium using yttria-stabilized zirconia (YSZ) balls. Subsequently, the milled powders were dried in an oven at 70°C and calcined at 1100°C for 2 hours. To prevent agglomeration, the calcined powders underwent an additional 12 h planetary milling process and were dried in an oven.

Preparation of Ceramics Slurry: The calcined STO powders were utilized to prepare a ceramic slurry. The STO powder was mixed with solvents (methyl-ethyl ketone + ethanol), dispersant (Triton), binder (polyvinyl butyral), and plasticizers (polyethylene glycol + benzyl butyl phthalate) in the required quantities. Table 1 provides the optimized composition of the slurry used. The ceramic slurry was prepared in two stages: (i) in the first stage, the STO powder was mixed with solvents and dispersant and ball milled for 24 h. (ii) Then, the binder and plasticizers were added and ball milled for 48 hours. Finally, a drop of cyclohexane was added and mixed for 3-4 h.

Table 1. Composition of STO slurry used

Materials	Content (wt. %)
Powder	65.9
Solvents	27.2
Dispersant	1.6
Plasticizers	2.3
Binder	2.3

Preparation of STO Tapes: The process of tape casting is depicted in Fig. 1. The STO slurry is prepared and then fed into the slurry holder of the tape casting machine. A doctor blade is used to adjust the height and thickness of the tape to the required dimensions. The tapes are cast onto a conveyor belt made of mylar sheet, which is controlled at a speed of 200-300 mm/min. A thin green tape is formed on the mylar sheet and then left to dry in the atmosphere. A green tape with a thickness of 75-80 μm is obtained, which is then sliced into dimensions of 14 x 14 mm. The sliced tapes are stacked on top of each other to form a thickness of 1.4 mm using a hydraulic press. The stacks are then sintered at 1450°C for 2 hours with slow rate heating and cooling cycles. After sintering, the thickness of the STO tape samples is reduced to 1.05 mm. The green and sintered STO tapes are shown in Fig. 2 (a and b).

Table 2. Particle size distribution of calcined STO powder

D_{10} (μm)	D_{50} (μm)	D_{90} (μm)	$D_{(3,2)}$ (μm)	$D_{(4,3)}$ (μm)	Specific surface area (m^2/kg)
0.81	2.02	5.48	1.61	3.04	589.9

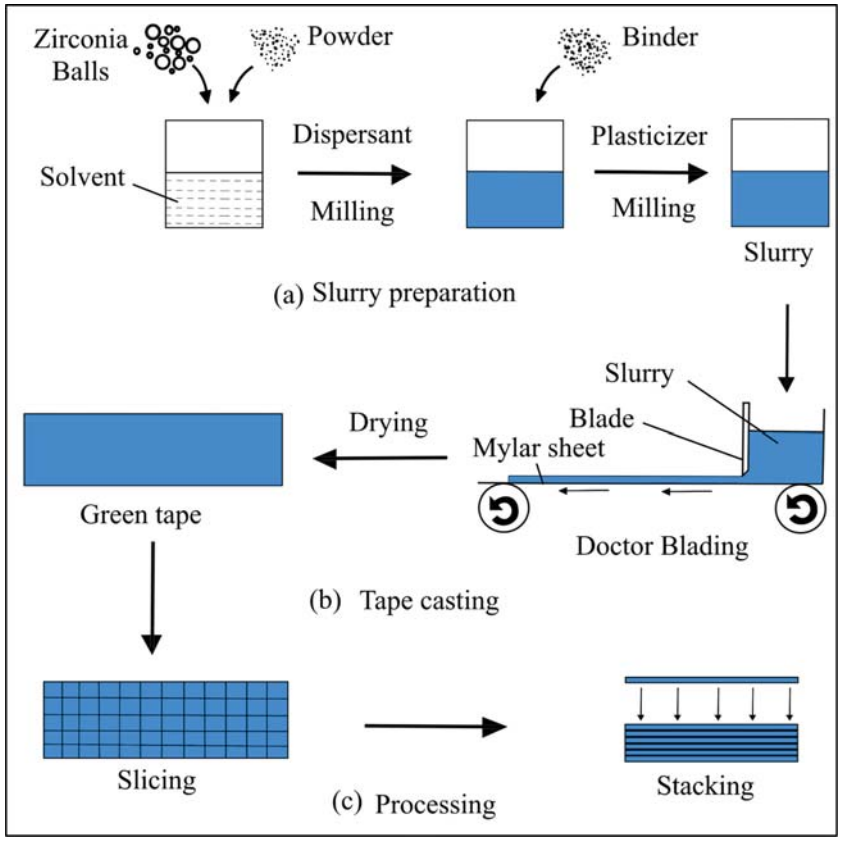

Fig. 1: Tape casting Method: (a) Slurry preparation (b) Tape casting (c) Processing (slicing and stacking)

Sample Characterization: The STO powders were analyzed using various techniques. X-ray diffraction patterns were obtained using a D8 Advance X-ray diffractometer by Bruker at a scanning rate of 1°/min. The particle size distribution was determined using a Mastersizer 3000 particle size analyzer from Malvern, UK, which utilizes laser diffraction to analyze the average particle size. The calcined STO powders were further analyzed using Fourier transform infrared (FTIR) spectroscopy with a PerkinElmer Frontier instrument. The IR spectrum was obtained in the scan range of 4000 cm^{-1} to 500 cm^{-1} with a scanning resolution of 4 cm^{-1}. Microstructure of the grains was obtained using a scanning electron microscope (SEM) from EVO 18 Research model from Carl Zeiss, Germany. The SEM samples were prepared by fine grade polishing with Al_2O_3 powders and then cleaned ultrasonically. To reveal the grains and grain boundaries, the samples were thermally etched at 1200 °C for 1 hour. Additionally, energy dispersive spectroscopy (EDS) analysis was conducted to determine the composition with respect to the atomic percentage of elements present in the samples. Area analysis was carried out to identify the elements. The direct current (DC) resistivity of the tape samples was measured using a 6517B electrometer from Keithley, Cleveland, at a constant voltage of 40 V with varying furnace temperatures up to 900°C. The sensitivity of the material was also assessed by determining the slope of the resistivity vs temperature graph.

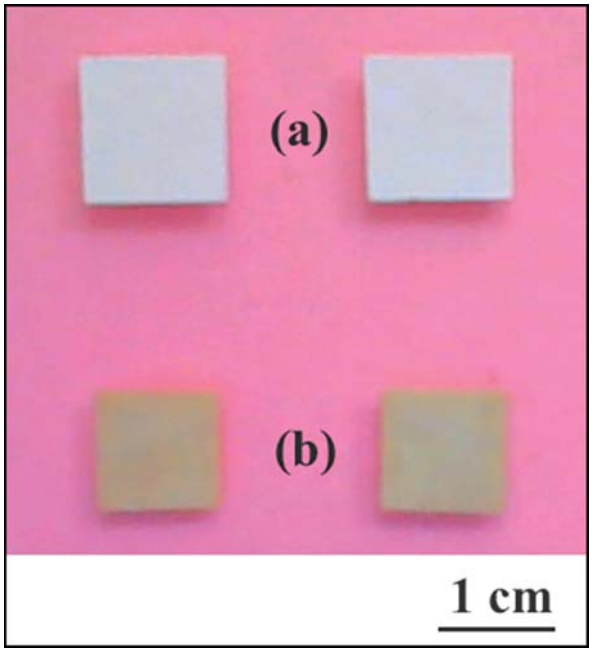

Fig. 2: STO tapes: (a) Green tape (b) sintered tapes (at 1450°C/ 2 h)

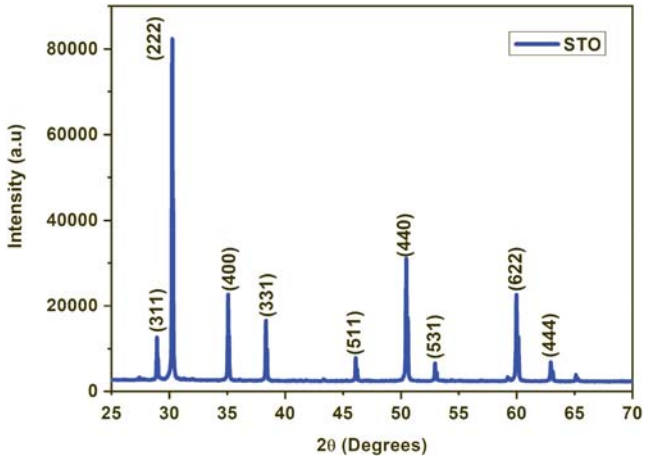

Fig. 3: XRD patterns of calcined STO powder

Results and Discussion

Fig. 3 displays the X-ray diffraction patterns of calcined STO powder. the X-ray diffraction patterns clearly indicate that the material exists as a single phase, with no evidence of a second phase compared to the standard powder diffraction file (JCPDS No.73–1699)[27]. The high intensity sharp peaks strongly suggest that the material is indeed crystalline in nature. Utilizing the Scherrer equation, $D = K \lambda / (\beta \cos \theta)$, where λ is the wavelength of Cu Kα (λ = 1.5406 Å) target, K is the shape factor (K = 0.89), β is full width half maximum and 2θ is the position of highest intensity peaks[28]. The average crystallite size was calculated to be approximately 63.42 nm.

The particle size distribution of calcined STO powder is illustrated in Fig. 4. The distribution, including D_{10}, D_{50} and D_{90} percentiles, is outlined in Table 2. The surface moment mean diameter of the particle, denoted as $D_{(3,2)}$, was observed to be 1.61 μm with a surface area of 589.9 m^2/kg. The FTIR spectrum of STO powder was obtained using the potassium bromide (KBr) pellet method and is displayed in Fig. 5. Transmittance peaks were observed at 3435 cm^{-1} and 682 cm^{-1}, indicating the presence of hydroxyl (O-H) bond and Ti-O bond, respectively. The O-H bond is attributed to the presence of moisture in the powders, while the Ti-O bond indicates the presence of titanium and oxygen bond in TiO6 octahedra.

The sintering process at 1450°C for 2 hours resulted in a maximum density of 96.42% (theoretical density of 6.305 g/cc). This temperature was selected based on previous studies on circular STO pellet samples[17]. The SEM micrograph of the sintered STO tape sample and the energy spectrum from EDS area analysis are presented in Fig. 6 (a and b). The average grain size was determined to be approximately 2.5 μm, exhibiting a globular morphology. The energy spectrum displayed distinct peaks with high intensities, corresponding to elements such as Sm, Ti, and O. The atomic percentages of these elements are detailed in Table 3, revealing that Ti constitutes approximately 19% and O comprises about 62% of the composition. The EDS data confirms the presence of $Sm_2Ti_2O_7$ material.

Table 3. Atomic percentage of elements from EDS area analysis of STO tapes

Elements	Atomic %
Sm	19.04
Ti	19.14
O	61.83

The DC resistivity of STO tape samples was measured while the temperature was changed from 100 to 900°C, as shown in Fig. 7. It was observed that the resistivity decreased linearly from 10^{10} - 10^6 Ω.cm within the temperature range of 400 to 900°C. These observations differ from previous studies where the circular pellets (bulk sample) showed a decrease in resistivity from 10^{13} - 10^6 Ω.cm in the range of 100 to 900°C[17]. Repeatability tests were also carried out for the samples, yielding similar results. The linear decrease in temperature may be due to the activation energy, which was calculated using the Arrhenius Equation to establish the relationship between resistivity (ρ) and temperature (T)[29] . The equation is given as: $\rho = A \exp(-Ea/kT)$, where A is the pre-exponential factor and k is the Boltzmann constant ($8.617e^{-5}$ eV/K). The activation energy (Ea) was calculated from the Arrhenius plot, giving the value of Ea/k, where k is

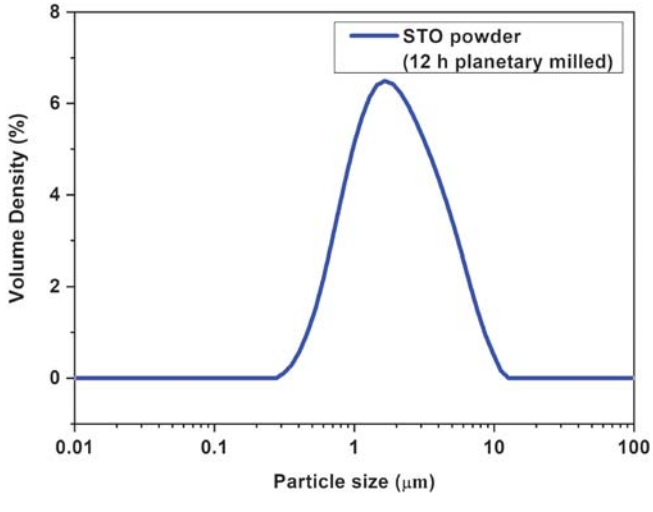

Fig. 4: Average particle size of calcined STO powder

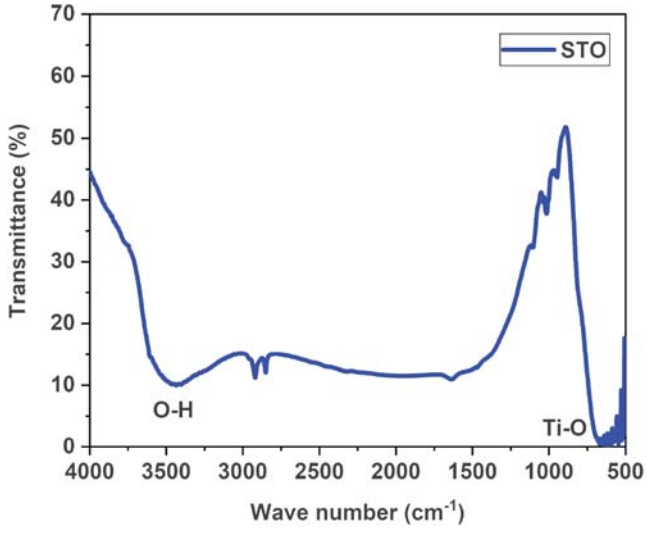

Fig. 5: FTIR spectrum of calcined STO powder

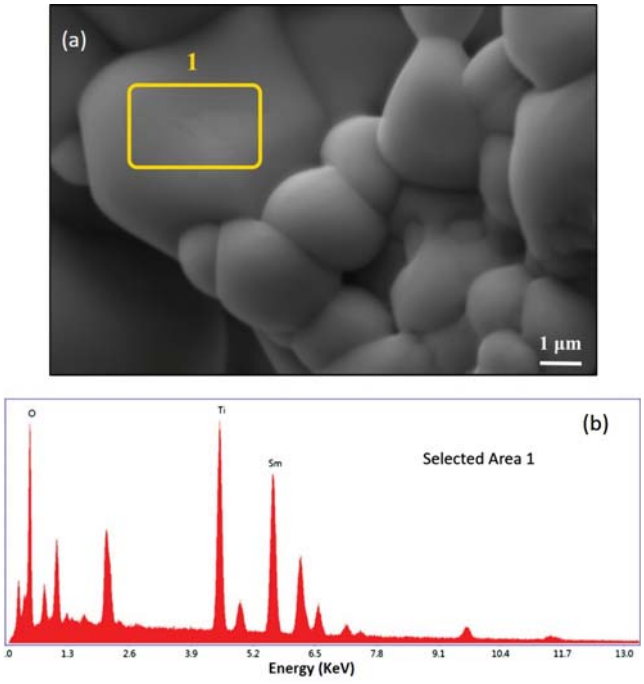

Fig. 6: (a) SEM image of sintered STO tape (b) EDS energy spectrum of area analysis

the Boltzmann constant. The activation energy for the lower temperature range from 100 to 400°C was 0.04 ± 0.02 eV (Ea_1), and for the higher temperature range from 500 to 900°C, it was 1.3 ± 0.07 eV (Ea_2). The higher activation energy for the temperatures from 500 to 900°C shows the intrinsic nature of the material, where the conductivity is high at elevated temperatures. Meanwhile, at lower temperatures (100 to 400°C), the activation energy is low, implying the extrinsic nature of the material due to low conductivity.

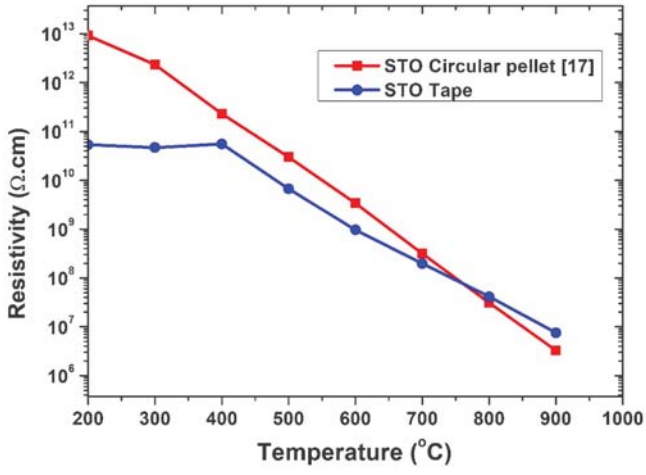

Fig. 7: DC electrical resistivity of sintered STO tape samples

The sensitivity 'S' is determined based on the output resistivity 'ρ' in relation to temperature 'T', which can be

Table 4. Comparison of resistivity and sensitivity of different sintered STO samples

Sample Type	Temperature (°C)	Resistivity (Ω.cm)	Sensitivity	References
Tapes	400-900	10^{10}-10^{6}	0.0175	Present work
Circular Pellets	100-900	10^{13}-10^{6}	0.0207	[17]

calculated using the equation $S = \rho/T$. A steeper slope on the graph indicates higher sensitivity of the material. The slope of the linear fit of natural logarithm of resistivity of STO tape was found to be 0.0175. Table 4 presents a comparison of resistivity and sensitivity between STO tape and circular STO pellet samples. It is observed that the pellet samples exhibit linear resistivity within a wide temperature range (100-900°C). The linear decrease in temperature from 400°C onwards for STO tapes may be attributed to the high activation energy up to 900°C, possibly due to the modified microstructure of the tapes during the tape casting process. Therefore, the tape samples can be utilized as temperature sensors for measuring temperatures above 400°C. Furthermore, the tape samples offer the advantage of producing thin tapes with the required dimensions. The tape casting method thus facilitates the fabrication of compact size sensors for high-temperature measurements.

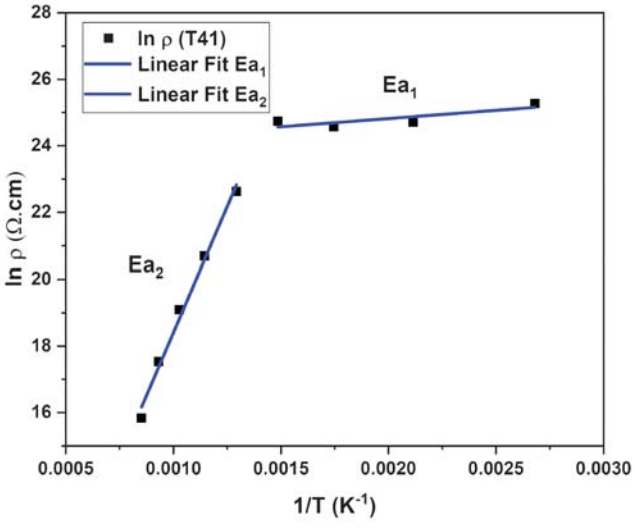

Fig. 8: Activation energy of sintered STO tape samples

Conclusions

The STO tapes were developed using the tape casting method and had a thickness of 80 ìm. The crystallite size of the calcined STO powders was found to be 63.42 nm, also confirming a single phase from XRD pattern. The

average particle size of the calcined STO powders was 1.61 μm. The sintered STO tapes displayed a percentage density of 96.42%, and with an average grain size of 2.5 μm measured from SEM micrographs. The DC electrical resistivity linearly decreased from 10^{10} to 10^{6} Ω.cm within the temperature range of 400 - 900 °C. The activation energy of the tape stacks was determined to be 0.04 ± 0.02 eV (Ea_1) from 100 - 400 °C and 1.3 ± 0.07 eV (Ea_2) from 500 - 900 °C. The sensitivity of the tape sample was observed to be 0.0175. Overall, this study demonstrates that the tape casting method can be utilized to produce thin tapes with desired dimensions, ultimately leading to the development of miniaturized high-temperature sensors.

Acknowledgements

The authors are grateful for the work done by the XRD and SEM departments of the Materials Science Division, CSIR-NAL. The authors also thank Department of Mechanical Engineering at RV College of Engineering for their encouragement in carrying out the work. ❒

References

1. F L Duan, Z Xie, Z Ji, and H Weng, *AIAA. J.* **58**, 41441-1445 (2020).
2. J Brübach, C Pflitsch, A Dreizler, and B Atakan, *Prog. Energ. Combust. Sci.* **39**, 37-60 (2013).
3. H Weng, F L Duan, Z Xie, S Liu, Z Ji, and Y Zhang, *IEEE Sens. J.* **20**, 12679-12683 (2020).
4. F L Duan, J Li, J Gao, G Ding, and X Cao, *J. Thermophys. Heat Transfer* **32,** 828-830 (2018).
5. Y Chen, Structure and properties of polymer-derived SiBCN ceramics Ph.D. Thesis (2012).
6. S Nilsson, H Feuk, and M Richter, *J. Lumin.* **256**, 119645 (2023).
7. I M Tougas, M Amani, and O J Gregory, *Sensors.* **13,** 15324-15347 (2013).
8. Z Cui, X Li, X Pan, G Chen, Y Li, J Lin, C Wu, X Liu, T Yang, T Yang, Z Hai, H Gonghan, Q Chen, and D Sun, *Sens. Actuators. A: Phys.* **332**, 113038 (2021).
9. Z Gao, Perovskite-Like Layered Structure $A_2B_2O_7$ Ferroelectrics and Solid Solutions, Ph.D. Thesis (2012).
10. H Ning, H Yan, and M J Reece, *J. Am. Ceram. Soc.* **93,** 1409-1413 (2010).
11. H Yan, H Ning, Y Kan, P Wang, and M J Reece, *J. Am. Ceram. Soc.* **92**, 2270-2275 (2009).
12. Z P Gao, H X Yan, H P Ning, and M J Reece, *Adv. Appl. Ceram.* **112,** 69-74 (2013).
13. P Sivagnanapalani, B Sahoo, and P K Panda, *ISSS J. Micro Smart Syst.* **8**, 25-30 (2019).
14. P Sivagnanapalani, B Sahoo, and P K Panda, *Ceram. Int.* **44**, 20348-20353 (2018).
15. N I Ansari, P Sivagnanapalani, V Sureshkumar, B W Shivaraj, and P K Panda, *J. Mater. Sci.: Mater. Electron.* **32**, 27422-27428 (2021).
16. P Sivagnanapalani, N I Ansari, and P K Panda, *Sens. Int.* **2**, 100093 (2021).
17. P Sivagnanapalani, and P K Panda, *Sens. Int.* **3**, 100200 (2022).
18. P R Roberge. Corrosion Engineering, Principals and Practice, McGraw-Hill, (2008).
19. H Yan, Tape casting and residual carbon in aluminum nitride, Rutgers The State University of New Jersey, School of Graduate Studies (1992).
20. G N Howatt, R G Breckenridge, and J M Brownlow, *J. Am. Ceram. Soc.* **30,** 237-242 (1947).
21. D Saha, R Giri, K K Mistry, and K Sengupta, *Sens. Actuators B: Chem.* **107,** 323-331 (2005).
22. R E Mistler, and E R Twiname, Tape casting: Theory and practice, *Wiley* (2000).
23. P K Panda, B Sahoo, M Chandraiah, S Raghavan, B Manoj, J Ramakrishna, and P Kiran, *J. Electron. Mater.* **44**, 4349-4353 (2015).
24. D E Bartolomeo, Kaabbuathong, M L Grilli, and E Traversa, *Solid State Ionics*, **171,** 173-181 (2004).
25. P K Sekhar, J Kysar, E L Brosha, and C R Kreller, *Sens. Actuators B: Chem.* **228,** 162-167 (2016).
26. A I Spitsin, A M Khramtsov, A G Segalla, A A Bush, and K E Kamentsev, *Ferroelectrics*, **539,** 134-140 (2019).
27. S Nanamatsu, M Kimura, and T Kawamura, *J. Phys. Soc. Jpn.* **38,** 817-824 (1975).
28. S Fatimah, R Ragadhita, D F Al Husaeni, and A B D Nandiyanto, *ASEAN J. Sci. Engg.* **2,** 65-76 (2022).
29. C Ang, R Guo, A S Bhalla, and L E Cross, *Integ. Ferroelectrics*, **42,** 419-431 (2002).